

Diagonal and off-diagonal thermal conduction with resonant phonon scattering in chiral Ni₃TeO₆

Heejun Yang¹, Xianghan Xu^{2,3}, Jun Han Lee⁴, Yoon Seok Oh⁴, Sang-Wook Cheong^{2,3}, and Je-Geun Park^{1,5,\$}

¹Department of Physics and Astronomy, Seoul National University, Seoul 08826, Republic of Korea

²Rutgers Center for Emergent Materials, Rutgers University, Piscataway, NJ, USA

³Department of Physics & Astronomy, Rutgers University, Piscataway, NJ, USA

⁴Department of Physics, Ulsan National Institute of Science and Technology, Ulsan 44919, Republic of Korea

⁵Institute of Applied Physics, Seoul National University, Seoul 08826, Republic of Korea

[\\$jgpark10@snu.ac.kr](mailto:jgpark10@snu.ac.kr)

Abstract

The coupling between phonon and magnon is ubiquitous in magnetic materials and plays a crucial role in many aspects of magnetic properties, most notably in spintronics. Yet, this academically and technologically interesting problem still poses a severe challenge to a general understanding of the issue in certain materials. We report that Ni₃TeO₆, a polar magnet, exhibits the clear evidence of significant magnon-phonon coupling in both longitudinal thermal conductivity (κ_{xx}) and thermal Hall coefficient (κ_{xy}). The Debye-Callaway model, a phenomenological description for phonon heat conduction, can explain the measured magnetic field dependence of $\kappa_{xx}(H)$: phonon scattering from spin fluctuation in the paramagnetic phase and additional scattering due to magnon-phonon coupling in the collinear antiferromagnetic phase. We further suggest that a similar approach could be applied to understand the finite κ_{xy} values in Ni₃TeO₆.

I. Introduction

Phonons are the dominant heat carrier and usually determine the overall thermal transport properties of most materials. The Debye-Callaway model [1], a standard phenomenological model, captures the essential temperature dependence. But there has been a long-standing question about how these phonons can interact with magnons, another fundamental quasiparticle in magnetic materials—this question goes back to the seminal paper by Kittel [2]. Despite the natural appeal of the idea, one has to wait for a considerable time before seeing actual experiments done with access to detailed measurements of both phonons and magnons [3,4].

These recent works primarily concern the case in which the bands of magnon and phonon get coupled to each other. But there can be another case of the magnon-phonon coupling, which is the resonant scattering of phonon via magnon [5–7]. The latter case is relatively rare because it requires a more stringent condition that magnons should have a large density of states at the right energy for the coupling to realize. Recently, the magnon-phonon coupling has renewed interest since the latest theoretical studies suggest that the magnon-phonon coupled term can produce nontrivial Berry curvature to its original Hamiltonian in several magnetic materials [8–11].

Observing Berry phase effects has been regarded as one piece of evidence for verifying the existence of novel quasiparticle [12,13], magnon topology [14–16], and topological phase transition [17] in magnetic insulators. For this reason, the thermal Hall effect (THE), the thermal analog of the electric Hall effect, was proposed as one experimental method to detect such topological effects of the spin system directly. In principle, phonon can also possess Berry curvature with possible phonon THE [18,19]. However, the typical size of phonon THE was expected to be negligible compared to its magnetic origin, as in $\text{Tb}_3\text{Ga}_5\text{O}_{12}$ [20], the first material showing phonon THE. Indeed, several successful THE measurements from magnon [21–24], nontrivial spin excitation in frustrated lattice [25–28], and Majorana fermion [29–31] were reported so far without considering the phonon effect.

However, there has been a new twist in these THE studies with a series of unexpectedly significant phonon THE: multiferroicity [32], quantum paraelectricity [33], structural domain [34], and pseudogap phase in cuprate [35–37]. These latest results all seem to point towards possibly genuine phonons effects. One common feature of these systems with the reported phonon THE is that the overall temperature dependence between thermal Hall coefficient (κ_{xy}) and longitudinal thermal conductivity (κ_{xx}) is quite similar to one another. With an apparently dominant phonon contribution to κ_{xx} for insulating system, the similarity between $\kappa_{xx}(T)$ and $\kappa_{xy}(T)$ (i.e. $\kappa_{xy}(T) \sim \kappa_{xx}(T)$) can be interpreted as that $\kappa_{xx}(T)$ and $\kappa_{xy}(T)$ would share the same origin, a likely candidate being phonons [34–38]. Moreover, recent studies showed that such a relationship, $\kappa_{xy}(T) \sim \kappa_{xx}(T)$, can also be found in other more exotic systems: e.g., the Kitaev quantum spin liquid candidate $\alpha\text{-RuCl}_3$ [39] and kagome antiferromagnet Cd-kapellasite [40]. They suggested that sizable κ_{xy} values found in the experiments might not be solely from Majorana fermion or other magnetic origin [39–41].

Unfortunately, however estimating the phonon contribution in κ_{xy} is still hard with detailed mechanisms for phonon Hall effect wanting [18,19,42–44].

Ni_3TeO_6 (NTO) can be one good example of the phonon THE as the specific heat of NTO remains nearly constant with various magnetic fields applied along the crystallographic c -axis [45], implying phonon dominant κ_{xx} in NTO [32]. It is also noteworthy that NTO is a polar magnet with other interesting properties: huge magnetoelectric effect [46] and phonon anomaly in antiferromagnetic (AFM) phase [47], indicating significant spin-phonon coupling. All these suggest a possible phonon THE in NTO. There are also two distinct magnetic structures below the Neel temperature (T_N): a collinear AFM structure with an easy axis along the c -axis [48] in the absence of the magnetic field (Fig. 1(a)) and an incommensurate conical spiral structure [49] of spin-flopped phase above the critical field ($\mu_0 H_c \sim 8.5$ T) applied along the c -axis [46] (Fig. 1(b)). We anticipate that this magnetic phase transition could affect both κ_{xx} and κ_{xy} , giving another clue for phonon THE.

In this paper, we report both in-plane κ_{xx} and κ_{xy} of NTO with the magnetic field applied along the c -axis up to 14 T. $\kappa_{xx}(T)$ seems to follow the conventional behavior of phonon thermal conductivity with pronounced suppression around T_N due to paramagnetic spin fluctuation. Observed $\kappa_{xy}(T)$ is still finite up to high temperature, two times of T_N , indicating that the phonon THE scenario is more appropriate than magnon. Moreover, the overall temperature dependence of $\kappa_{xy}(T)$ is similar to $\kappa_{xx}(T)$, further suggesting the phonon THE in NTO. On the other hand, $\kappa_{xx}(H)$ shows two opposite-field dependences between the paramagnetic and AFM phases: slight increasing $\kappa_{xx}(H)$ in $T > T_N$, and more complex decreasing $\kappa_{xx}(H)$ in $T < T_N$. We used the Debye-Callaway theory to model the resonant phonon scattering process [1,50–53] from magnon to find that it gives a fair phenomenological understanding of κ_{xx} for $T < T_N$ and $H < H_c$. We propose that such magnon-phonon interaction would also be a dominant factor for κ_{xy} .

II. Experimental Methods

Ni_3TeO_6 single crystals were grown by a flux method modified from a previous report [54]. Stoichiometric Na_2CO_3 and TeO_2 powders were mixed and sintered at 850 °C for 10 hours to make a Ni_3TeO_6 polycrystalline precursor. For single crystal growth, powders of $\text{Ni}_3\text{TeO}_6 : \text{V}_2\text{O}_5 : \text{TeO}_2 : \text{NaCl} : \text{KCl} = 1 : 1.5 : 3 : 3 : 1.5$ in the molar ratio were mixed and filled into a platinum crucible. The crucible was kept at 850 °C for 10 hours before being slowly cooled to 500 °C at a 2 °C/h rate, after which the heaters were switched off for natural cooling to room temperature. Ni_3TeO_6 crystals with a typical size of 1.5 mm * 1.5 mm * 0.1 mm were mechanically separated from the product after overnight bathing in hot 1M NaOH. The chirality of Ni_3TeO_6 crystals was determined by a polarized-light optical microscope [55]. Fig. 1(c) and

(d) show that the Ni_3TeO_6 sample used in this study consists of a single chiral domain.

Thermal conductivity was measured using a homemade setup, which works based on a conventional steady-state method with one heater and three thermometers [33, 56]. To minimize error from strong magnetic fields and self-heating of thermometers, homemade SrTiO_3 capacitors were adopted as thermometers with careful in-situ calibration [56]. As shown in Fig. 1(e), heat current and the magnetic field are applied along the ab -plane and the c -axis of the sample, respectively. Three thermometers measure temperature differences along x ($\Delta T_x = T_1 - T_2$) and y ($\Delta T_y = T_3 - T_2$) directions, simultaneously. Since the typical size of κ_{xy} is three orders of magnitude smaller than κ_{xx} and longitudinal contact misalignment is inevitable, we antisymmetrized ΔT_y to get true thermal Hall response (δT_y) using the following relation, $\delta T_y(+H) = \frac{\Delta T_y(+H) - \Delta T_y(-H)}{2}$.

III. Data and Analysis

Fig. 2(a) shows the dc magnetic susceptibility (χ_{dc}) measured with 0.2 T parallel to the c -axis after zero-field cooling. With decreasing temperature from 300 K, χ_{dc} follows the Curie-Weiss law exhibiting a single peak near 52 K and converges toward zero rapidly as the temperature gets further reduced. We determined T_N of NTO as 52 K from the sharp peak in $d\chi_{dc}/dT$ (inset of Fig. 2(a)), consistent with the previous report [46]. The black straight line in Fig. 2(a) is obtained from the Curie-Weiss fitting between 150 and 300 K. The experimental $1/\chi_{dc}$ starts to deviate from the fitting below 100 K, indicating short-range correlations for $T_N < T < 100$ K.

Fig. 2(b) displays $\kappa_{xx}(H = 0, 14 \text{ T})$ and $\kappa_{xy}(H = 14 \text{ T})$ as a function of temperature. For $T < T_N$, $\kappa_{xx}(T)$ follows the typical phonon thermal conductivity with a peak around 30 K [57]. However, $\kappa_{xx}(T)$ starts to increase gradually slightly above T_N , which does not match with the decreasing nature of typical phonon conductivity at higher temperatures. Interestingly, $\kappa_{xx}(T)$ is restored back to the normal behavior as expected of phonon for $T > 130$ K. This broad increase of $\kappa_{xx}(T)$ seen for $T_N < T < 130$ K is difficult to understand especially as there exists strong spin fluctuations in the paramagnetic phase [58–61], as found in the susceptibility. These spin fluctuations would be expected to suppress, not boost, thermal conductivity. On the other hand, a magnetic field produces negligible effects to $\kappa_{xx}(T)$ for $T > T_N$ whereas there is overall suppression in $\kappa_{xx}(T)$ for $T < T_N$.

As regards THE, we found $\kappa_{xy}(T)$ to behave negatively linear with magnetic fields right up to two times of T_N . For $T > T_N$, finite $\kappa_{xy}(T)$ was observed without further changes even at 170 K, the highest temperature our setup can access: our SrTiO_3 thermometers lose sensitivity at the higher temperature. It is well known that magnon Hall conductivity disappears rapidly above a magnetic ordering temperature [21–24]. Therefore, we can assume that $\kappa_{xy}(T)$ in NTO should originate from other sources for $T > T_N$: for which phonon is a natural candidate. Upon cooling from T_N , the magnitude of $\kappa_{xy}(T)$ increases rapidly with a peak

around 30 K before being suppressed at lower temperatures. Hence, both $\kappa_{xx}(T)$ and $\kappa_{xy}(T)$ show a very similar temperature dependence in NTO. This similarity again reinforces our conclusion that the phonon Hall effect is most likely to be dominant in the AFM phase of NTO, as in Ref. [34–38].

The detailed field dependences of both $\kappa_{xx}(H)$ and $\kappa_{xy}(H)$ are shown in Fig. 3 (a) and (b), respectively. For $T > T_N$, $\kappa_{xx}(H)/\kappa_{xx}(0)$ increases by less than 1 %, which can be interpreted as phonon scattering due to spin fluctuations in the paramagnetic state: the magnetic field aligns the spin moment, thereby lowering the phonon scattering [23,26,27,40,62]. On the other hand, the overall decreasing behavior of $\kappa_{xx}(H)/\kappa_{xx}(0)$ seen for $T < T_N$ indicates that dominant phonon scattering mechanism in the ordered phase is different from those in the paramagnetic phase. As temperature lowers, $\kappa_{xx}(H)$ behaves in a more complex manner, showing an upturn and a sharp suppression in $\kappa_{xx}(H)$ seen around $\mu_0 H \sim 8.5$ T, the critical field (H_c) of the spin-flop transition [46]. This anomaly can be interpreted as an abrupt change of phonon scattering during the magnetic phase transition, further evidence of strong spin-phonon coupling in NTO. On the other hand, $\kappa_{xy}(H)$ shows linear field dependence for all the measured temperatures (Fig. 3(b)). It is noticeable that at lower temperatures $\kappa_{xy}(H)$ also shows an anomaly at the spin-flop transition, which is similar to $\kappa_{xx}(H)$.

According to the Boltzmann transport equation, phonon thermal conductivity (κ_{xx}^{ph}) can be expressed in terms of specific heat (C), group velocity (v), and relaxation time (τ) of phonon: $\kappa \sim \frac{1}{3} C v^2 \tau$. Since the specific heat shows negligible magnetic field effect in NTO [45], we can conclude that τ should play a more dominant role in the field dependence of κ_{xx}^{ph} . Hence, we adopted the Debye-Callaway model of Eq. (1), a phenomenological model [1], to analyze the field dependence of $\kappa_{xx}(H)$ in the ordered phase of NTO:

$$\kappa_{xx}^{ph} = \frac{k_B^4}{2\pi^2 v \hbar^3} T^3 \int_0^{\frac{T_D}{T}} \frac{x^4 e^x}{(e^x - 1)^2} \tau(\omega, T) dx \quad (1)$$

where $\tau^{-1}(\omega, T)$ is the scattering rate of phonon, T_D is the Debye temperature, ω is the frequency of phonon and $x = \frac{\hbar\omega}{k_B T}$ is the phonon energy normalized by the thermal energy. The average sound velocity (v) is estimated from the Debye model using the following relation: $T_D = v \frac{\hbar}{k_B} (6\pi^2 n)^{1/3}$, where n is the number of atoms per unit volume. $\tau^{-1}(\omega, T)$ can then be approximated by a sum of different scattering sources

$$\tau^{-1}(\omega, T) = \frac{v}{d} + A_0 \omega + A_1 \omega^4 + A_2 \omega^2 T \exp\left(-\frac{T_D}{bT}\right) + \tau_{res}^{-1} \quad (2)$$

The first four terms in Eq. (2) represent phonon scattering from sample boundary, linear defects, point defects, and umklapp process, respectively; all these terms are, a priori, field-independent. For field-dependent κ_{xx} , we thus considered resonant phonon scattering process (τ_{res}^{-1}) as described in Fig. 4(a). In this scenario, the low-lying magnon bands having a higher density of states (DoS) split linearly under the magnetic field with an energy difference

of $\hbar\omega_{res}$. We note that our hypothesis of the low-lying magnon band with a large DoS is consistent with the recent spin waves measurements [49]. This process then allows phonons to be scattered with magnons having the specific energy of $\hbar\omega_{res}$ [57]. We chose an empirical formula for τ_{res}^{-1} of Eq. (3), which has been shown to successfully explain κ_{xx} in several complex magnetic insulator [50–53]:

$$\tau_{res}^{-1} = R \frac{\omega^4}{(\omega^2 - \omega_{res}^2)^2} \frac{\exp\left(-\frac{\hbar\omega_{res}}{k_B T}\right)}{1 + \exp\left(-\frac{\hbar\omega_{res}}{k_B T}\right)} \quad (3)$$

where R indicates the strength of resonant phonon scattering.

We further note that our scenario of the resonant phonon scattering process makes sense, given that the decreasing $\kappa_{xx}(H)$ happens only below T_N . In this explanation of the linearly split magnon band, as in Fig. 4(b), the magnon mode (\mathcal{E}_{\pm}) in the collinear easy-axis AFM phase can be written as Eq. (4) under the magnetic field applied along the easy-axis [63]. As a result, we can get $\hbar\omega_{res} = 2g\mu_B\mu_0 H$, where μ_B is Bohr magneton and $g = 2.26$ is the g-factor of NTO [64].

$$\mathcal{E}_{\pm}(H) = \mathcal{E}(H = 0) \pm g\mu_B\mu_0 H \quad (4)$$

Although d , b , T_D , A_0 , A_1 , A_2 , and R in Eq. (2) are in principle free parameters, we can put further constraints on several parameters (d , b and T_D) for a minimum model. First, we can fix d as 1 mm, the shortest in-plane dimension of the sample: d represents the phonon mean free path due to collisions from the sample boundary. Next, b , the characteristic constant of the phonon dispersion, can be fixed using a conventional value of $2\sqrt[3]{N} \sim 6.21$, where N is the number of atoms in a unit cell [58,65,66]. To determine the appropriate value of T_D , we fitted the specific heat data taken from previous studies [48,67]; using the Debye-Einstein model, we estimate $T_D = 470$ K. As a result, the free parameters can be reduced to the only four A_0 , A_1 , A_2 , and R : all of which indicate the strength of each scattering process.

The best-fitting result is shown as black dashed curves in Fig. 3(a), using $A_0 = 3.29 \times 10^{-4}$, $A_1 = 6.44 \times 10^{-43} \text{ s}^3$, $A_2 = 4.04 \times 10^{-18} \text{ s} \cdot \text{K}^{-1}$, and $R = 1.77 \times 10^8 \text{ s}^{-1}$. These values are comparable to previous studies, which also employed the Debye-Callaway model in their analysis [50–53,58]. The calculated $\kappa_{xx}^{ph}(H)/\kappa_{xx}^{ph}(0)$ reproduces well the overall behavior of $\kappa_{xx}(H)/\kappa_{xx}(0)$ for $T < T_N$ and $H < H_c$, including the upturn seen for $T < 10$ K. It is not surprising to find, though, that the fitting breaks down for $T \geq T_N$ since the magnon will be no longer well-defined in the paramagnetic phase. From this exercise, we can conclude that the resonant phonon scattering model may as well be a reasonable explanation for $\kappa_{xx}(H)$ in NTO. However, we admit that our model cannot explain the data in the higher field region $\kappa_{xx}(H > H_c)$. It is mainly due the fact that the magnetic structure and Hamiltonian are not known in the spin-flopped phase.

Using the same parameters, we also calculated $\kappa_{xx}^{ph}(T)$ at zero-field shown as a black solid curve in Fig. 2(b). We can see that the measured $\kappa_{xx}(T)$ is suppressed from $\kappa_{xx}^{ph}(T)$ in the temperature range of $T_N < T < 130$ K. As previous thermal transport studies pointed out, paramagnetic spin fluctuations could scatter phonons off, resulting in flat-like $\kappa_{xx}(T)$ [58,65,68]. Thus, we can conclude that the significant spin fluctuation and magnon strongly affect the phonon heat transport in NTO.

IV. Discussion

We now like to discuss the implications of our THE work. As there is no good model for the phonon THE yet, we can only make general observations by comparing it with other materials having finite κ_{xy} . First, the mechanism proposed for the phonon THE in non-magnetic insulator SrTiO₃ is hard to be applied to NTO because it requires a substantial dielectric constant ($\epsilon \sim 10^4$) with structural domain [34,44] or quantum paraelectricity [33]: none of which can be considered for NTO. Instead, we conjecture that in the paramagnetic phase, the phonon Hall effect in NTO originates from the secondary effect of significant spin-phonon coupling [20,62]. We also noticed that the size of $\kappa_{xy}(T)$ rapidly increases just below T_N (Fig. 2(b)) and $\kappa_{xy}(H)$ starts to show a hump-like behavior at H_c (Fig. 3(b)); all of which indicates that magnetically ordered phase affects κ_{xy} significantly. Since the relation $\kappa_{xy}(T) \sim \kappa_{xx}(T)$ implies that both κ_{xx} and κ_{xy} are highly correlated and magnon-phonon scattering model describes κ_{xx} well, we suggest that the magnon-phonon interaction is also a dominant factor for κ_{xy} in the AFM phase.

We also anticipate that the magnon-phonon picture presented here could be used to understand other recent thermal Hall experiments properly. For example, both $\kappa_{xx}(T)$ and $\kappa_{xy}(T)$ in Cu₃TeO₆ are very similar to NTO [38], with suppression in $\kappa_{xx}(T)$ around T_N [69]. Moreover, $\kappa_{xy}(T)$ in Cu₃TeO₆ starts to increase quickly following the relation $\kappa_{xy}(T) \sim \kappa_{xx}(T)$ for $T < T_N$ [38]. According to this idea, the rapid increased $\kappa_{xy}(T)$ in the AFM phase could originate from magnon-phonon interaction in Cu₃TeO₆ [69]. Furthermore, we can find more common features in $\kappa_{xx}(H)$ and $\kappa_{xy}(H)$ of Fe₂Mo₃O₈, another polar magnet with a collinear AFM phase along the *c*-axis accompanying the spin-flip transition [32]. We believe that our model can also be used to explain the data in Fe₂Mo₃O₈.

To summarize, we measured both κ_{xx} and κ_{xy} of an insulating polar magnet Ni₃TeO₆. We observed finite negative κ_{xy} up to two times of T_N and a similar temperature dependence between κ_{xy} and κ_{xx} , which indicates phonon dominant thermal Hall effect in Ni₃TeO₆. The collinear AFM phase has κ_{xx} well described by the Debye-Callaway model with additional resonant phonon scattering from the magnon band. We suggest that the same origin governs both κ_{xx} and κ_{xy} : spin-phonon coupling for $T > T_N$ and magnon-phonon interaction for $T < T_N$.

We expect that the phonon Hall effect from magnon-phonon interaction could apply to other insulating magnets in the magnetically ordered phase.

Acknowledgment

We want to thank Ysun Choi for the helpful discussion. The work at SNU was supported by the Leading Researcher Program of Korea's National Research Foundation (Grant No. 2020R1A3B2079375). J.H.L. and Y.S.O. acknowledge support from the Basic Science Research Programs through the National Research Foundation of Korea (NRF) (NRF-2020R1A2C1009537).

Reference

- [1] J. Callaway, Phys. Rev. **113**, 1046 (1959).
- [2] C. Kittel, Phys. Rev. **110**, 836 (1958).
- [3] J. Oh *et al.*, Nat. Commun. **7**, 13146 (2016).
- [4] T. Kim *et al.*, J. Phys. Soc. Japan **88**, 081003 (2019).
- [5] G. S. Dixon, Phys. Rev. B **21**, 2851 (1980).
- [6] G. S. Dixon, V. Benedict, and J. E. Rives, Phys. Rev. B **21**, 2865 (1980).
- [7] J. A. H. M. Buys and W. J. M. de Jonge, Phys. Rev. B **25**, 1322 (1982).
- [8] X. Zhang *et al.*, Phys. Rev. Lett. **123**, 167202 (2019).
- [9] S. Park and B.-J. Yang, Phys. Rev. B **99**, 174435 (2019).
- [10] G. Go, S. K. Kim, and K.-J. Lee, Phys. Rev. Lett. **123**, 237207 (2019).
- [11] S. Zhang *et al.*, Phys. Rev. Lett. **124**, 147204 (2020).
- [12] H. Katsura, N. Nagaosa, and P. A. Lee, Phys. Rev. Lett. **104**, 066403 (2010).
- [13] J. Nasu, J. Yoshitake, and Y. Motome, Phys. Rev. Lett. **119**, 127204 (2017).
- [14] R. Matsumoto and S. Murakami, Phys. Rev. Lett. **106**, 197202 (2011).
- [15] S. A. Owerre, J. Phys. Condens. Matter **28**, 386001 (2016).
- [16] K.-S. Kim *et al.*, Phys. Rev. B **100**, 064412 (2019).
- [17] R. R. Neumann *et al.*, Phys. Rev. Lett. **128**, 117201 (2022).
- [18] L. Zhang *et al.*, Phys. Rev. Lett. **105**, 225901 (2010).
- [19] T. Qin, J. Zhou, and J. Shi, Phys. Rev. B **86**, 104305 (2012).
- [20] C. Strohm, G. L. J. A. Rikken, and P. Wyder, Phys. Rev. Lett. **95**, 155901 (2005).
- [21] Y. Onose *et al.*, Science (80-.). **329**, 297 (2010).
- [22] T. Ideue *et al.*, Phys. Rev. B **85**, 134411 (2012).
- [23] M. Hirschberger *et al.*, Phys. Rev. Lett. **115**, 106603 (2015).
- [24] H. Zhang *et al.*, Phys. Rev. Lett. **127**, 247202 (2021).
- [25] M. Hirschberger *et al.*, Science (80-.). **348**, 106 (2015).
- [26] D. Watanabe *et al.*, Proc. Natl. Acad. Sci. **113**, 8653 (2016).
- [27] H. Doki *et al.*, Phys. Rev. Lett. **121**, 097203 (2018).
- [28] M. Yamashita *et al.*, J. Phys. Condens. Matter **32**, 074001 (2020).
- [29] Y. Kasahara *et al.*, Phys. Rev. Lett. **120**, 217205 (2018).
- [30] Y. Kasahara *et al.*, Nature **559**, 227 (2018).

- [31] T. Yokoi *et al.*, *Science* (80-.). **373**, 568 (2021).
- [32] T. Ideue *et al.*, *Nat. Mater.* **16**, 797 (2017).
- [33] S. Sim *et al.*, *Phys. Rev. Lett.* **126**, 015901 (2021).
- [34] X. Li *et al.*, *Phys. Rev. Lett.* **124**, 105901 (2020).
- [35] G. Grissonnanche *et al.*, *Nature* **571**, 376 (2019).
- [36] G. Grissonnanche *et al.*, *Nat. Phys.* **16**, 1108 (2020).
- [37] M.-E. Boulanger *et al.*, *Nat. Commun.* **11**, 5325 (2020).
- [38] L. Chen *et al.*, arXiv:2110.13277 (2021).
- [39] É. Lefrançois *et al.*, arXiv:2111.05493 (2021).
- [40] M. Akazawa *et al.*, *Phys. Rev. X* **10**, 041059 (2020).
- [41] Y. Hirokane *et al.*, *Phys. Rev. B* **99**, 134419 (2019).
- [42] M. Mori *et al.*, *Phys. Rev. Lett.* **113**, 265901 (2014).
- [43] T. Saito *et al.*, *Phys. Rev. Lett.* **123**, 255901 (2019).
- [44] J.-Y. Chen, S. A. Kivelson, and X.-Q. Sun, *Phys. Rev. Lett.* **124**, 167601 (2020).
- [45] J. W. Kim *et al.*, *Phys. Rev. Lett.* **115**, 137201 (2015).
- [46] Y. S. Oh *et al.*, *Nat. Commun.* **5**, 3201 (2014).
- [47] M. O. Yokosuk *et al.*, *Phys. Rev. B* **92**, 144305 (2015).
- [48] I. Živković *et al.*, *J. Phys. Condens. Matter* **22**, 056002 (2010).
- [49] J. Lass *et al.*, *Phys. Rev. B* **101**, 054415 (2020).
- [50] A. V Sologubenko *et al.*, *Phys. Rev. Lett.* **84**, 2714 (2000).
- [51] R. Hentrich *et al.*, *Phys. Rev. Lett.* **120**, 117204 (2018).
- [52] R. Hentrich *et al.*, *Phys. Rev. B* **102**, 235155 (2020).
- [53] X. Hong *et al.*, *Phys. Rev. B* **104**, 144426 (2021).
- [54] R. Sankar *et al.*, *Dalt. Trans.* **42**, 10439 (2013).
- [55] X. Wang *et al.*, *APL Mater.* **3**, 076105 (2015).
- [56] H.-L. Kim *et al.*, *Rev. Sci. Instrum.* **90**, 103904 (2019).
- [57] R. Berman, *Thermal Conductions in Solids* (Oxford University Press, 1976).
- [58] P. A. Sharma *et al.*, *Phys. Rev. Lett.* **93**, 177202 (2004).
- [59] L. D. Casto *et al.*, *APL Mater.* **3**, 041515 (2015).
- [60] A. Haglund, PhD thesis, Univ. Tennessee, Knoxville. (2019).
- [61] Y. Liu *et al.*, *Adv. Funct. Mater.* **2105111**, 2105111 (2022).
- [62] K. Sugii *et al.*, *Phys. Rev. Lett.* **118**, 145902 (2017).

- [63] S. M. Rezende, A. Azevedo, and R. L. Rodríguez-Suárez, *J. Appl. Phys.* **126**, 151101 (2019).
- [64] J. Zupan, D. Kolar, and V. Urbanč, *Mater. Res. Bull.* **6**, 1353 (1971).
- [65] D. Bansal *et al.*, *Phys. Rev. B* **95**, 054306 (2017).
- [66] G. A. Slack, in *Solid State Phys. - Adv. Res. Appl.* (1979), pp. 1–71.
- [67] R. Dawar *et al.*, *J. Nucl. Mater.* **493**, 219 (2017).
- [68] C. Chiorescu, J. J. Neumeier, and J. L. Cohn, *Phys. Rev. Lett.* **101**, 257202 (2008).
- [69] S. Bao *et al.*, *Phys. Rev. B* **101**, 214419 (2020).

Figures

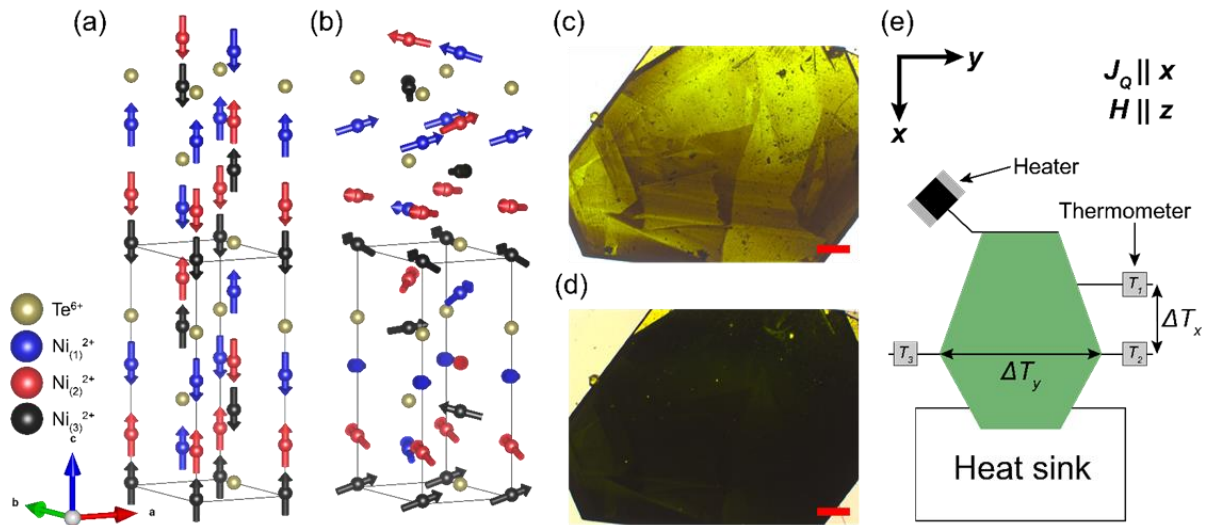


Figure 1 Magnetic structure of Ni_3TeO_6 and schematic of thermal transport experimental setup (a) Collinear antiferromagnetic structure of the low-field phase. (b) The incommensurate conical spiral magnetic structure of the spin-flopped phase, as suggested in Ref. [49]. (c) and (d) Images of Ni_3TeO_6 samples taken using a transmission polarized optical microscope. Scale bars are 200 μm . (c) The sample shows transparent green color with parallel polarizer and analyzer. (d) Slight rotation of the analyzer makes the chiral domain to be visible. The overall dark color indicates a single chiral domain in the sample. (e) Schematic of thermal transport experimental setup. Heat current (J_Q) and magnetic field (H) are applied along the ab -plane and the c -axis of the sample, respectively.

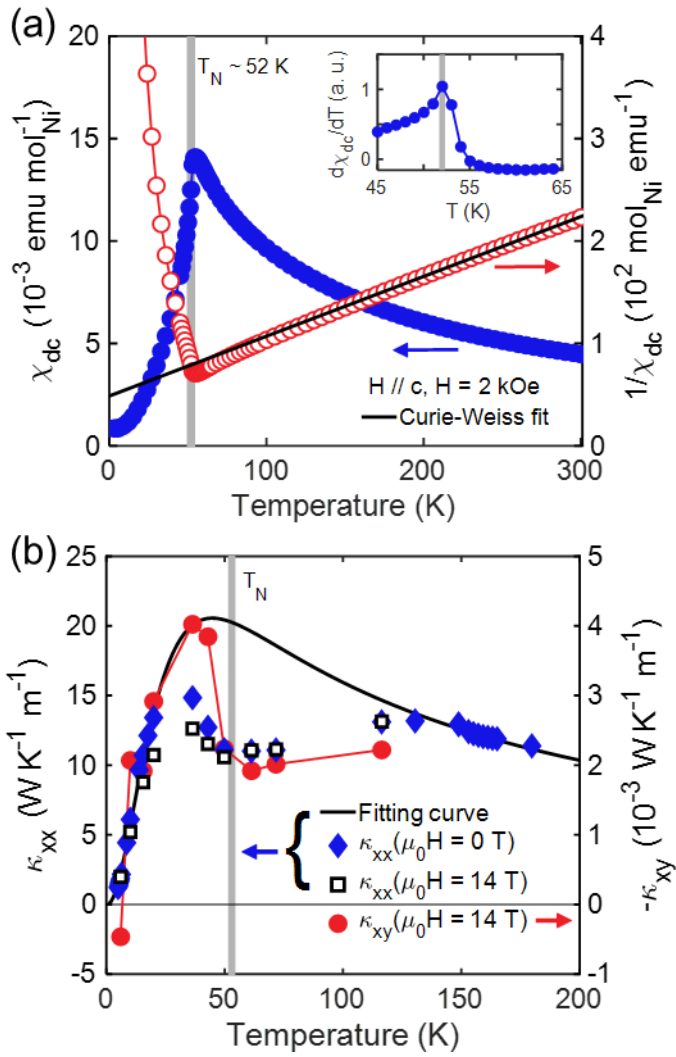


Figure 2 **Measured dc magnetic susceptibility (χ_{dc}) along the c-axis, longitudinal thermal conductivity (κ_{xx}) and thermal Hall coefficient (κ_{xy}) as a function of temperature.** (a) Blue filled and red open circles display χ_{dc} and $1/\chi_{dc}$, respectively. The inset shows $d\chi_{dc}/dT$ with a clear transition peak near 52 K, indicating an antiferromagnetic phase transition. A solid black line is obtained from the Curie-Weiss law fitting. (b) Blue diamond and open square show κ_{xx} at 0 and 14 T, respectively. Red circle shows $-\kappa_{xy}$ at a magnetic field of 14 T. The solid black curve is obtained from the Debye-Callaway model by fitting the zero-field κ_{xx} data.

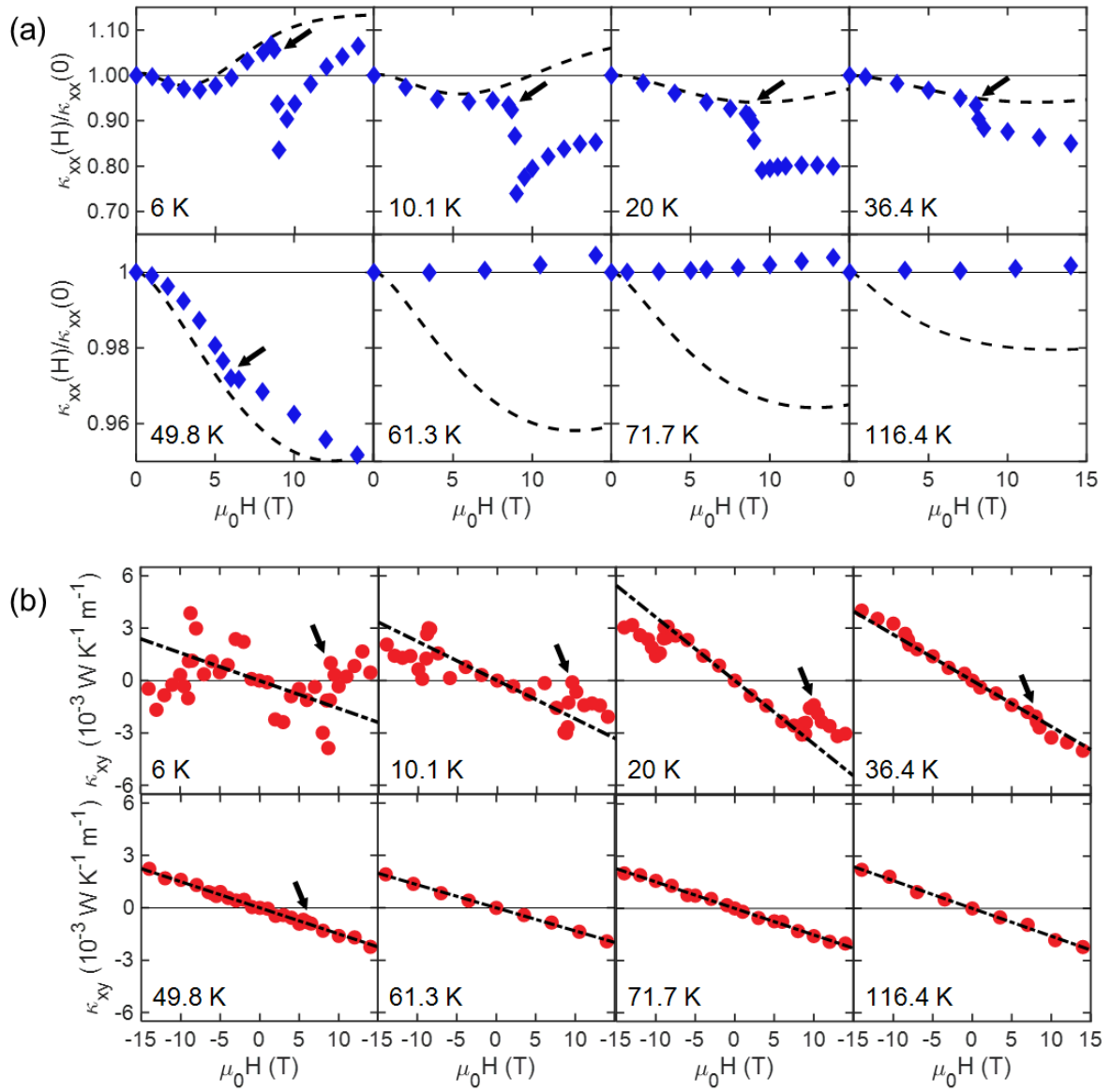


Figure 3 **Measured magneto-thermal conductivity ($\kappa_{xx}(H)/\kappa_{xx}(0)$) and thermal Hall coefficient (κ_{xy}) as a function of magnetic field.** (a) Blue diamond shows $\kappa_{xx}(H)/\kappa_{xx}(0)$ at various temperature points. Black dashed curves are obtained from the Debye-Callaway model. (b) The red circle shows the field dependence of κ_{xy} at various temperatures. Black dash-dotted lines are guides to the eye clarifying the dominant linearity of κ_{xy} , especially in the low-field collinear antiferromagnetic phase. Black arrows indicate a sharp anomaly on κ_{xx} and κ_{xy} due to the spin-flop transition.

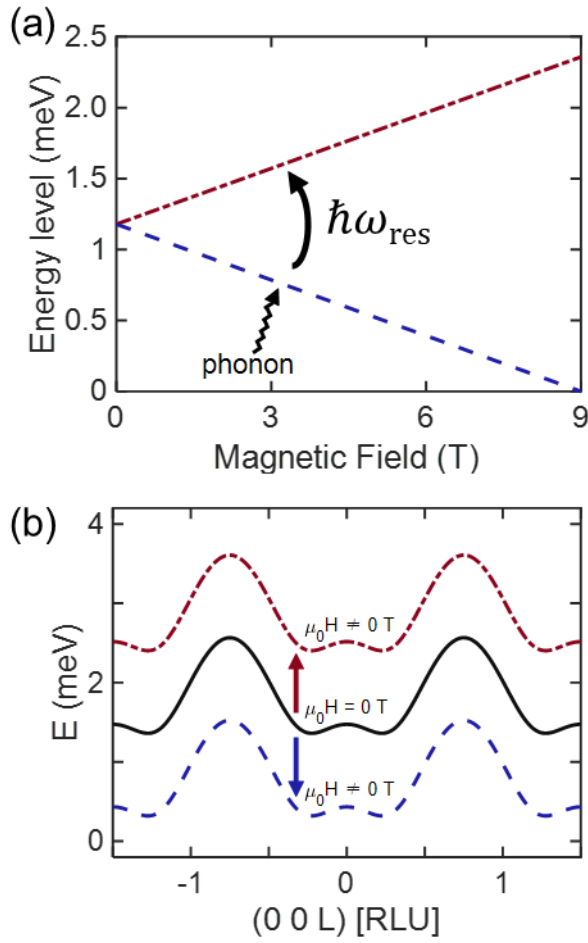


Figure 4 **Schematic of resonant phonon scattering process and effective magnon dispersion of Ni_3TeO_6 in collinear antiferromagnetic phase.** (a) Two energy levels in low-lying magnon bands get linear split under the magnetic field. $\hbar\omega_{res}$ is the energy difference between lower and upper energy levels of the magnon bands. Blue dashed and red dash-dotted lines represent the lower and upper energy levels. The following process can describe resonant phonon scattering: a lower energy level absorbs phonon with the energy of $\hbar\omega_{res}$, resulting in excitation of the upper level [57]. (b) Effective magnon dispersion in the low-field phase was obtained from Ref. [49]. The black curve shows the dispersion at a zero magnetic field. With a magnetic field, the magnon dispersion starts to split. The red-dotted and blue dashed curves show the dispersion with a finite field.